MATHEMATICAL MODELING AND COMPUTING, Vol. 8, No. 4, pp. 691–704 (2021)

Modeling Computing Mathematical

TSDT theory for free vibration of functionally graded plates with various material properties

Janane Allah M., Belaasilia Y., Timesli A., El Haouzi A.

Hassan II University of Casablanca, National Higher School of Arts and Crafts (ENSAM Casablanca), 20670 Casablanca, Morocco

(Received 23 May 2021; Accepted 7 June 2021)

In this work, an implicit algorithm is used for analyzing the free dynamic behavior of Functionally Graded Material (FGM) plates. The Third order Shear Deformation Theory (TSDT) is used to develop the proposed model. In this contribution, the formulation is written without any homogenization technique as the rule of mixture. The Hamilton principle is used to establish the resulting equations of motion. For spatial discretization based on Finite Element Method (FEM), a quadratic element with four and eight nodes is adopted using seven degrees of freedom per node. An implicit algorithm is used for solving the obtained problem. To study the accuracy and the performance of the proposed approach, we present comparisons with literature and laminate composite modeling results for vibration natural frequencies. Otherwise, we examine the influence of the exponent of the volume fraction which reacts the plates "P-FGM" and "S-FGM". In addition, we study the influence of the thickness on "E-FGM" plates.

Keywords: *third order shear deformation theory (TSDT), nonlinear dynamic analysis, laminate composite, functionally graded material (FGM).*

2010 MSC: 65D05, 65D30, 65N30, 74A40, 74D10 **DOI:** 10.23939/mmc2021.04.691

1. Introduction

Since a long time composite materials play a major role in the overall industry (Automotive, aeronautics, civil engineering, etc). These industries are in permanent search of performance in terms of production gain, lifespan, maintenance and functionality. Currently, most research and development activities in structural applications have mainly focused on areas of joining two basic constituents, such as ceramic and metal. The joint between two constituents with two different materials encounters a problem on the structural interfaces. In 1987, the researchers proposed to use Functionally Graded Materials (FGMs). These particular composite materials having a gradual and continuous variation of the volume fractions of each constituent. In this kind of materials, properties vary from one point to another eliminating interface problems. In FGM materials, material fraction varies continuously through the thickness to have a material with two facets made up of ceramic and metal. The change in material fraction is made between these two facets by laws describing the manufacturing process of the FGM. Many benefits are expected from using this class of FGM. For example, the ceramic face can provide high wear resistance, while the metal face offers the high hardness. Thus, these materials are highly desirable for automotive applications because of the wear resistance and high hardness. The use of FGM materials in the automotive industry is still limited at the moment, due to the high cost of production. However, the material is used in very important parts of vehicles, where the use of this kind of material is justified by scientific reasons. Present applications include pistons, cylinder liners for diesel engine, leaf springs, combustion chambers, transmission shafts, shock absorbers, some parts of the bodywork, etc. Also, FGMs are used in bodywork coatings, such as graduated coatings with particles, for improved rigidity of cars. Research activity on FGMs is centered around the calculation of residual stresses, analysis and study of the temperature evolution in FGMs (thermal stresses), calculation of interfacial stresses in FGMs, modeling of stresses and strains in the different vibration studies of FGMs structures.

In the following, we present some scientific research on FGMs. Vinh et al. (2021) [1] proposed a modified plate theory of shear strain to analyze the free vibration of rectangular P-FGM plates. Using the equilibrium of forces equations, the relationship between the bending and shear parts is established, so that the displacement fields and the equation of the modified theory of plates contain only a single unknown variable. Auada et al. (2019) [2] investigated an isogeometric analysis of the FGM plates. The kinematic model is based on the Reissner-Mindlin theory for flexural and shear strains and the von Karman theory for nonlinear membrane strains. Isogeometric formulation is applied to study buckling and post-buckling of FGM plates. Kim et al. (2019) [3] presented a semi-analytical approach to study the nonlinear dynamic response and the vibration of an eccentrically oblique rigid plate in FGM resting on elastic foundation. Fu et al. (2018) [4] analyzed the sound transmission loss through corrugated core FGM sandwich plates filled with porous material. They considered two types of FGM sandwich structures, one with FGM face sheets and homogeneous ceramic or metal core, and the other is reversed with homogeneous face sheets and FGM core. Sharma et al. (2021) [5] studied the free vibrations of the two-dimensional P-FGM square plate. The natural frequencies are calculated for various boundary conditions using COMSOL-5.5 finite element software. Kar and Srinivas (2020) [6] used the materials modeling and finite element analysis to study the behavior of the P-FGM hydroxyapatite/titanium plate under thermo-mechanical loads. Unlike other studies in which the plates are separately exposed to thermal or mechanical loads, a simultaneous analysis is performed in this work. Katili et al. (2021) [7] performed a static and dynamic (free vibration) analysis of P-FGM plates using an efficient quadrilateral finite element based on the discrete shear projection method (DSPM). Zheng et al. (2021) [8] developed a hybrid meshless/displacement discontinuity method for FGM Reissner's plate with cracks. In addition, Multi-term extended Kantorovich method (MTEKM) and the classical plate theory are used by Hassan and Kurgan (2020) [9] to examine the bending of thin skew FGM plate embedded in the Winkler elastic foundation under uniformly distributed transverse load. Various configurations of boundary conditions are considered. Yang et al. (2020) [10] analyzed the postbuckling of multi-directional perforated FGM plates using NURBS-based on isogeometric analysis and finite cell method. TSDT and von Karman nonlinear assumptions are used to determinate the nonlinear deformation of plate, where shear correction factors are not needed in this model. Minh et al. (2021) [11] introduced the high order shear strain theory (HSDT) to calculate the free vibration of cracked plates (P-FGM) resting on elastic Pasternak foundations. A linearly variable thickness and a crack in the center are considered for the rectangular plate. Li et al. (2021) [12] studied composite laminated and FGM plates using higher-order shear deformation theories with a novel unified plate model. The parameters of free vibration of plates of cracked P-FGM materials whose thickness varies nonlinear according to the symmetrical function of parabola under temperature studied. Minh and Duc (2020) [13] investigate the free vibration parameters of cracked FGM plates under temperature using the symmetric parabola function for nonlinear varying thickness. Tran et al. (2021) [14] used ES-MITC3 element and prediction of artificial neural network to examine free vibrations of P-FGM plates in the thermal environment embedded in elastic foundations. Timesli (2021) [15] investigated analytical modeling of buckling behavior of porous FGM cylindrical shell embedded within an elastic foundation uisng Donnell shell theory. In the work of Bourihane et al. (2020) [16], the free vibration and forced nonlinear dynamic behavior of plate material (P-FGM) are analyzed using TSDT. FGM plates operate as a laminated composite, and the power-law governs the variation of the material properties of FGM. The resulting equations of motion established according to Hamilton's principle.

In the present work, we are interested to the vibrations of FGM plates using TSDT and FEM. We suppose that the material properties change continuously through the thickness of the plate using the different laws which govern the variation of materials namely: the exponential law "E-FGM", the power-law "P-FGM", and the "S-FGM" sigmoid law. The equations of motion obtained by applying the Hamilton principle and the fundamental frequencies calculated by solving the equations governing the eigenvalue problem. Firstly for validation, we compare the results of the "P-FGM" plate obtained with those of the literature. Afterward, we examine the influence of the exponent of the volume fraction which governs "P-FGM" and "S-FGM" plates. Then we study the influence of the thickness on the "E-FGM" plates with different boundary conditions.

2. The laws of the variation of the material properties depending on the thickness of FGM plates

The material gradation methods of the variation of the material properties of FGM plates are given as follows.

2.1. Material properties of P-FGM plates (Power law gradation)

Many researchers use a power law function "P-FGM" to describe the material properties of materials with graduated functionality. Once the local volume fraction $V(z)_m$ is defined, the material properties of "P-FGM" plate can be determined by the rule of mixtures:

- Young's Modulus:

$$E(z) = (E_c - E_m) \times V(z) + E_m, \quad (1)$$

- Poisson's ratio:

$$\nu(z) = (\nu_c - \nu_m) \times V(z) + \nu_m, \quad (2)$$

- Mass Density:

$$\rho(z) = (\rho_c - \rho_m) \times V(z) + \rho_m, \quad (3)$$

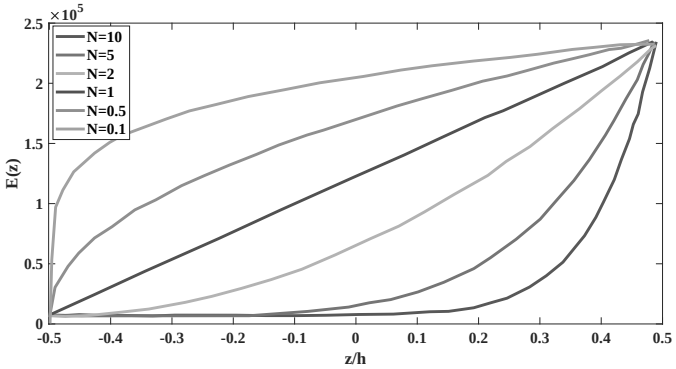

Fig. 1. Variation of Young's modulus in a P-FGM plate.

where E_c, v_c and ρ_c define the properties of the ceramic material and E_m, v_m and ρ_m define the properties of the metal material. The expression of volume fraction of the P-FGM is given by a power law function:

$$V(z) = \left(\frac{z}{h} + \frac{1}{2}\right)^N, \quad (4)$$

where h is the thickness of the plate and N $(0 \leqslant N \leqslant \infty)$ is an exponent of the volume fraction which represents the variation of the material through the thickness of the layer in FGM. The variation of Young's modulus through the thickness of the P-FGM plate is shown in Fig. 1.

2.2. Material properties of E-FGM plates (Exponential law gradation)

For E-FGM plates, the exponential function is used to describe the material properties.

- Young's Modulus:

$$E(z) = E_c \times \exp\left(B\left(z + \frac{h}{2}\right)\right) \quad (5)$$

with $B = \frac{1}{h}\ln\left(\frac{E_c}{E_m}\right)$,

- Poisson's ratio:

$$v(z)_{=} v_c \times \exp\left(B\left(z + \frac{h}{2}\right)\right) \quad (6)$$

with $B = \frac{1}{h}\ln\left(\frac{v_c}{v_m}\right)$,

- Mass Density:

$$\rho(z) = \rho_c \times \exp\left(B\left(z + \frac{h}{2}\right)\right) \quad (7)$$

with $B = \frac{1}{h}\ln\left(\frac{\rho_c}{\rho_m}\right)$.

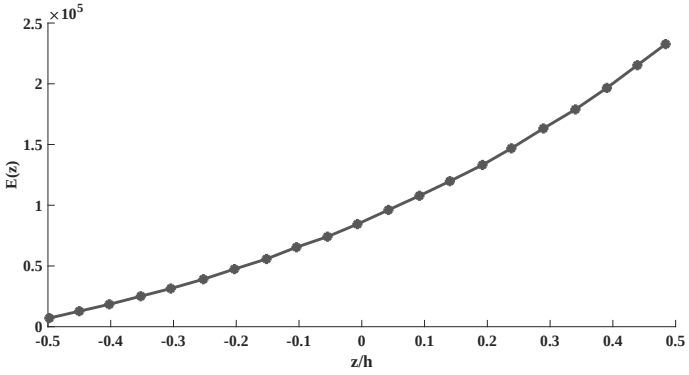

Fig. 2. Variation of Young's modulus in a E-FGM plate.

The variation of Young's modulus through the thickness of the E-FGM plate is shown in Fig. 2.

2.3. Material properties of S-FGM plates (Sigmoid law gradation)

In power and exponential laws, stress concentrations appear in one of the interfaces, this problem is overcome by the sigmoid law [17] which combines two power laws. The expressions of this law for unidirectional S-FGM are given by:

- Young's Modulus:
$$E(z) = (E_c - E_m) \times V(z) + E_m, \tag{8}$$
- Poisson's ratio:
$$\nu(z) = (\nu_c - \nu_m) \times V(z) + \nu_m, \tag{9}$$
- Mass density:
$$\rho(z) = (\rho_c - \rho_m) \times V(z) + \rho_m. \tag{10}$$

The expression of volume fraction is given by power laws in the form:

$$\begin{cases} V(z) = 1 - \frac{1}{2}\left(\frac{\frac{h}{2}-z}{\frac{h}{2}}\right)^N & \text{for} \quad 0 \leqslant z \leqslant h/2, \\ V(z) = \frac{1}{2}\left(\frac{\frac{h}{2}-z}{\frac{h}{2}}\right)^N & \text{for} \quad -h/2 \leqslant z \leqslant 0. \end{cases} \tag{11}$$

3. Mathematical formulation

3.1. Mechanical characteristics and Kinematics

Considering a FGM plate in Cartesian coordinates as shown in Fig. 3 with the following geometric characteristics: length b, width a and thickness h. The displacement of each point of the FGM plate is defined by $\langle U\rangle^T = \langle u, v, w\rangle^T$ which is correspond to the displacement of a point between the reference state and the deformed state of the plate. The displacement components u, v, and w are defined according to the coordinates (x, y, z). The components u_0 and v_0 correspond to the displacement in the middle plane $(x, y, 0)$. The middle plane is positioned in $z = 0$ with $u(x, y, 0) = u_0(x, y)$ and $v(x, y, 0) = v_0(x, y)$. The mechanical properties of plate $E(z)$, $\nu(z)$, and $\rho(z)$ depend on the coordinate z and vary from values E_c, ν_c, and ρ_c) to values E_m, ν_m, and ρ_m. Note that E_c, ν_c, and ρ_c are the properties of the top face ($z = h/2$) of the shell and E_m, ν_m, and ρ_m are the properties of the bottom face ($z = -h/2$) as shown in Figs. 3 and 4.

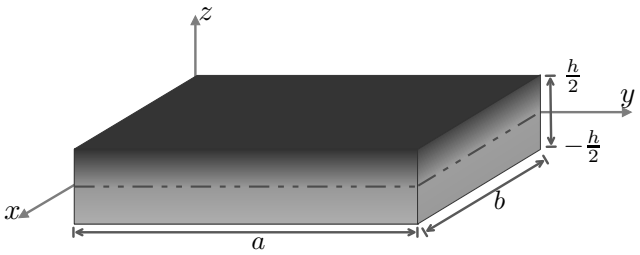

Fig. 3. FGM plate in Cartesian coordinates.

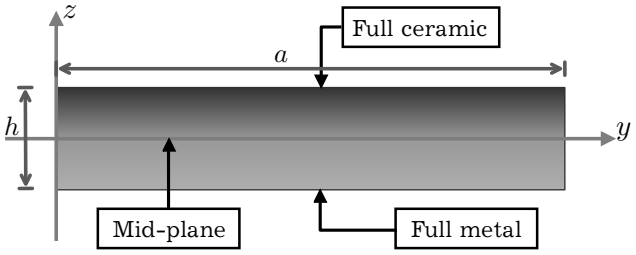

Fig. 4. Material properties through the thickness of the FGM plate.

To adapt TSDT for elasticity problems, we assume a non-linear elastic behavior of the plate. The field of displacements of a point M of the plate is written in the form:

$$U(M)=\begin{cases} u(x,y,z,t)=u_0(x,y)-z\frac{\partial w_0(x,y)}{\partial x}+f(z)\varphi_x(x,y),\\ v(x,y,z,t)=v_0(x,y)-z\frac{\partial w_0(x,y)}{\partial y}+f(z)\varphi_y(x,y),\\ w(x,y,z,t)=w_0(x,y), \end{cases} \tag{12}$$

where u_0, v_0, and w_0 are the membrane displacements. $\varphi_x(x,y)$ and $\varphi_y(x,y)$ are given by:

$$\begin{cases} \varphi_x(x,y)=\frac{\partial w_0(x,y)}{\partial x}+\theta_x,\\ \varphi_y(x,y)=\frac{\partial w_0(x,y)}{\partial y}+\theta_y, \end{cases} \tag{13}$$

where θ_x and θ_y are the rotations around the axis x and y.

For Reddy's TSDT $f(z)=z(1-cz^2)$ with $c=\frac{4}{3h^2}$, hence displacement field can express as:

$$U(M)=\begin{cases} u(x,y,z,t)=u_0(x,y)+z\theta_x-c\,z^3\big(\frac{\partial w_0(x,y)}{\partial x}+\theta_x\big),\\ v(x,y,z,t)=v_0(x,y)+z\theta_y-c\,z^3\big(\frac{\partial w_0(x,y)}{\partial y}+\theta_y\big),\\ w(x,y,z,t)=w_0(x,y), \end{cases} \tag{14}$$

3.2. Deformation field

The strain tensor of Green–Lagrange γ is related to the displacement field by the following relation:

$$\gamma_{ij}=\frac{1}{2}\left(\frac{\partial U_i}{\partial x_j}+\frac{\partial U_j}{\partial x_i}\right)+\frac{1}{2}\sum_{k=1}^{3}\frac{\partial U_k}{\partial x_i}\frac{\partial U_k}{\partial x_j}. \tag{15}$$

The small displacement assumption allows us to write the strain tensor of Green–Lagrange in the following vector form:

$$\{\gamma_{ij}\}=\begin{Bmatrix}\gamma_{xx}\\2\gamma_{xy}\\2\gamma_{xz}\\\gamma_{yy}\\2\gamma_{yz}\end{Bmatrix}=\begin{Bmatrix}\frac{\partial u}{\partial x}\\\frac{\partial u}{\partial y}+\frac{\partial v}{\partial x}\\\frac{\partial u}{\partial z}+\frac{\partial w}{\partial x}\\\frac{\partial v}{\partial y}\\\frac{\partial v}{\partial y}+\frac{\partial w}{\partial y}\end{Bmatrix}+\frac{1}{2}\begin{Bmatrix}\big(\frac{\partial u}{\partial x}\big)^2+\big(\frac{\partial v}{\partial x}\big)^2+\big(\frac{\partial w}{\partial x}\big)^2\\2\big(\frac{\partial u}{\partial x}\frac{\partial u}{\partial y}+\frac{\partial v}{\partial x}\frac{\partial v}{\partial y}+\frac{\partial w}{\partial x}\frac{\partial w}{\partial y}\big)\\2\big(\frac{\partial u}{\partial x}\frac{\partial u}{\partial z}+\frac{\partial v}{\partial x}\frac{\partial v}{\partial z}+\frac{\partial w}{\partial x}\frac{\partial w}{\partial z}\big)\\\big(\frac{\partial u}{\partial y}\big)^2+\big(\frac{\partial w}{\partial y}\big)^2+\big(\frac{\partial w}{\partial y}\big)^2\\2\big(\frac{\partial u}{\partial y}\frac{\partial u}{\partial z}+\frac{\partial v}{\partial y}\frac{\partial v}{\partial z}+\frac{\partial w}{\partial y}\frac{\partial w}{\partial z}\big)\end{Bmatrix}. \tag{16}$$

This tensor can be written as follows:

$$\{\gamma\}=\{\varepsilon\}+z*\{\kappa\}-3c*z^2\{\varphi\}-cz^3\{\psi\} \tag{17}$$

with $\{\varepsilon\}$ is given by:

$$\{\varepsilon\}=\begin{Bmatrix}\frac{\partial u_0}{\partial x}\\\frac{\partial v_0}{\partial y}\\\frac{\partial u_0}{\partial y}+\frac{\partial v_0}{\partial x}\\\frac{\partial w_0}{\partial z}+\theta_x\\\theta_y+\frac{\partial w_0}{\partial y}\end{Bmatrix}+\frac{1}{2}\begin{Bmatrix}\big(\frac{\partial u_0}{\partial x}\big)^2+\big(\frac{\partial v_0}{\partial x}\big)^2+\big(\frac{\partial w_0}{\partial x}\big)^2\\\big(\frac{\partial u_0}{\partial y}\big)^2+\big(\frac{\partial v_0}{\partial y}\big)^2+\big(\frac{\partial w_0}{\partial y}\big)^2\\2\big(\frac{\partial u_0}{\partial x}\frac{\partial u_0}{\partial y}+\frac{\partial v_0}{\partial x}\frac{\partial v_0}{\partial y}+\frac{\partial w_0}{\partial x}\frac{\partial w_0}{\partial y}\big)\\2\big(\frac{\partial u_0}{\partial x}\theta_x+\frac{\partial v_0}{\partial x}\theta_y\big)\\2\big(\frac{\partial u_0}{\partial y}\theta_x+\frac{\partial v_0}{\partial y}\theta_y\big)\end{Bmatrix} \tag{18}$$

or in short form:

$$\{\varepsilon\}=[H_1]\{\theta\}+\frac{1}{2}[A(\theta)]\{\theta,\} \tag{19}$$

where the displacement gradient vector $\{\theta\}$ is written as follows:

$$\{\theta\}^T=\langle u_{0,x},v_{0,x},w_{0,x},u_{0,y},v_{0,y},w_{0,y},\theta_x,\theta_y,\theta_{x,x},\theta_{y,x},\theta_{x,y},\theta_{y,y},w_{,xx},w_{0,yy},w_{0,xy}\rangle \tag{20}$$

and the matrices $[H_1]$ and $[A(\theta)]$ are given by:

$$[H_1] = \begin{bmatrix} 1 & 0 & 0 & 0 & 0 & 0 & 0 & 0 & \dots \\ 0 & 0 & 0 & 0 & 1 & 0 & 0 & 0 & \dots \\ 0 & 1 & 0 & 1 & 0 & 0 & 0 & 0 & \dots \\ 0 & 0 & 1 & 0 & 0 & 0 & 1 & 0 & \dots \\ 0 & 0 & 0 & 0 & 0 & 1 & 0 & 1 & \dots \end{bmatrix} \tag{21}$$

and

$$[A(\theta)] = \begin{bmatrix} 0 & 0 & w_{0,x} & 0 & 0 & 0 & 0 & 0 & \dots \\ 0 & 0 & 0 & 0 & 0 & w_{0,y} & 0 & 0 & \dots \\ 0 & 0 & w_{0,y} & 0 & 0 & w_{0,x} & 0 & 0 & \dots \\ 0 & 0 & 0 & 0 & 0 & 0 & 0 & 0 & \dots \\ 0 & 0 & 0 & 0 & 0 & 0 & 0 & 0 & \dots \end{bmatrix}. \tag{22}$$

3.3. Behavior law

The second Piola–Kirchhoff stress tensor S and the Green-Lagrange strain tensor γ are connected by the following relation:

$$\gamma_{i,j} = \frac{1+v(z)}{E(z)} S_{i,j} - \frac{v(z)}{E(z)} S_{kk}\delta_{i,j}, \tag{23}$$

where $\delta_{i,j}$ is the Kronecker symbol. This relation can be written in the matrix form:

$$\begin{Bmatrix} S_{xx} \\ S_{yy} \\ S_{xy} \\ S_{xz} \\ S_{yz} \end{Bmatrix} = \big[D(z)\big] \begin{Bmatrix} \gamma_{xx} \\ \gamma_{yy} \\ 2\gamma_{xy} \\ 2\gamma_{xz} \\ 2\gamma_{xy} \end{Bmatrix}, \tag{24}$$

where $[D(z)]$ is the matrix of the elastic behavior,

$$\big[D(z)\big] = \frac{E(z)}{1-v(z)^2} \begin{bmatrix} 1 & v(z) & 0 & 0 & 0 \\ v(z) & 1 & 0 & 0 & 0 \\ 0 & 0 & \frac{1-V(z)}{2} & 0 & 0 \\ 0 & 0 & 0 & \frac{1-V(z)}{2} & 0 \\ 0 & 0 & 0 & 0 & \frac{1-V(z)}{2} \end{bmatrix}. \tag{25}$$

4. Application of Hamilton's principle

The equations of motion are derived from Hamilton's principle which is given by the following expression:

$$\delta H = \delta \int_{t0}^{t1} (T-P)dt = 0, \tag{26}$$

where T is the kinetic energy, P is the total potential energy, H is the Hamiltonian of the system, t_0 and t_1 are the initial and final time, respectively, and dt is the time variation. The kinetic energy T is given by:

$$T = \frac{1}{2} \int \rho(z) \{\dot{U}(M)\}^2 d\Omega, \tag{27}$$

where $\{\dot{U}(M)\}$ is velocity field. The variation of the kinetic energy is then given by:

$$\delta T = \int \rho(z) \{\delta\dot{U}\}^T \{\dot{U}\} d\Omega. \tag{28}$$

Integrating the kinetic energy from time t_0 to time t_1 one can obtain:

$$\int_{t_0}^{t_1} \delta T\, dt = \int_{t_0}^{t_1} \int \rho(z)\{\delta\dot{U}\}^T\{\dot{U}\}\, d\Omega\, dt, \tag{29}$$

$$\int_{t_0}^{t_1} \delta T\, dt = \underbrace{\int_{t_0}^{t_1} \int \rho(z)\{\delta\dot{U}\}^T\{\dot{U}\}\, d\Omega\, dt\Big|_{t_0}^{t_1}}_{a} - \underbrace{\int_{t_0}^{t_1} \int \rho(z)\{\delta U\}^T\{\ddot{U}\}\, d\Omega\, dt}_{b}, \tag{30}$$

where the first term "a" is zero because $\delta U = 0$ at times $t = t_0$ and $t = t_1$. Hence the expression of kinetic energy becomes:

$$\delta T = -\int \rho(z)(\ddot{u}\delta u + \ddot{v}\delta v + \ddot{w}\delta w)\, d\Omega, \tag{31}$$

where $\ddot{u}$, $\ddot{v}$, $\ddot{w}$ are the components of the acceleration vector and δu, δv, δw are the variation of displacements at point M. Subsequently, to facilitate the calculation of the operations, we set $\beta_j = \theta_j + w_j$, where $j = x, y$, and $M_i = \int z^i \rho(z) dz$ where $i = 0, 1, 2, 3, 4, 6$ and M_i is a component of the mass matrix. The variation of the kinetic energy is then given by:

$$\begin{aligned}\delta T = -\int \Big[& M_0(\ddot{u}\delta u + \ddot{v}\delta v + \ddot{w}\delta w) + M_1(\ddot{u}\delta\theta_x + \ddot{v}\delta\theta_y + \ddot{\theta}_x\delta u + \ddot{\theta}_y\delta v) \\ & + M_2(\ddot{\theta}_x\delta\theta_x + \ddot{\theta}_y\delta\theta_y) - cM_3(\ddot{u}\delta\beta_x + \ddot{v}\delta\beta_x + \ddot{\beta}_x\delta u + \ddot{\beta}_y.\delta v) \\ & - cM_4(\ddot{\theta}_x\delta\beta_x + \ddot{\theta}_y\delta\beta_y + \ddot{\beta}_x\delta\theta_x + \ddot{\beta}_y\delta\theta_y) + c^2M_6(\ddot{\beta}_x\delta\beta_x + \ddot{\beta}_y\delta\beta_y)\Big] dS\end{aligned} \tag{32}$$

or by the following compact form:

$$\delta T = -\int \langle\delta U\rangle[M]\{\ddot{U}\}\, dS, \tag{33}$$

where

$$\langle\delta U\rangle = \langle\delta u, \delta v, \delta w, \delta\beta_x, \delta\beta_y, \delta\theta_x, \delta\theta_y\rangle \tag{34}$$

and

$$[M] = \begin{bmatrix} M_0 & 0 & 0 & -CM_3 & 0 & M_1 & 0 \\ 0 & M_0 & 0 & 0 & -CM_3 & 0 & M_1 \\ 0 & 0 & M_0 & & 0 & 0 & 0 \\ -CM_3 & 0 & 0 & C^2M_6 & 0 & -CM_4 & 0 \\ 0 & -CM_3 & 0 & 0 & C^2M_6 & 0 & -CM_4 \\ M_1 & 0 & 0 & -CM_4 & 0 & M_2 & 0 \\ 0 & M_1 & 0 & 0 & -CM_4 & 0 & M_2 \end{bmatrix}. \tag{35}$$

The variation of the total potential energy is written as follows:

$$\delta P = \delta W_d + \delta W_{ext}, \tag{36}$$

where δW_d is the variation of strain energy and δW_{ext} is the variation of work done by the external force. δW_d is given by:

$$\delta W_d = \int \{\delta\gamma\}^T\{S\}\, d\Omega, \tag{37}$$

which allows to obtain:

$$\begin{aligned}\delta W_d = \int \Big(& \langle\delta\varepsilon\rangle[D_0]\{\varepsilon\} + \langle\delta\kappa\rangle[D_1]\{\varepsilon\} - 3c\langle\delta\varphi\rangle[D_2]\{\varepsilon\} \\ & - c\langle\delta\psi\rangle[D_3]\{\varepsilon\} + \langle\delta\varepsilon\rangle[D_1]\{\kappa\} + \langle\delta\kappa\rangle[D_2]\{\kappa\} - 3c\langle\delta\varphi\rangle[D_3]\{\kappa\} \\ & - c\langle\delta\psi\rangle[D_4]\{\kappa\} - 3\langle\delta\varepsilon\rangle[D_2]\{\varphi\} - 3c\langle\delta\kappa\rangle[D_3]\{\varphi\} \\ & + 9c^2\langle\delta\varphi\rangle[D_4]\{\varphi\} + 3c^2\langle\delta\psi\rangle[D_5]\{\varphi\} - c\langle\delta\varepsilon\rangle[D_3]\{\psi\} - c\langle\delta\kappa\rangle[D_4]\{\psi\} \\ & + 3c^2\langle\delta\varphi\rangle[D_5]\{\psi\} + c^2\langle\delta\psi\rangle[D_6]\{\psi\}\Big) dS,\end{aligned} \tag{38}$$

where

$$[D_i] = \int z^i [D(z)]\, dz \quad \text{with} \quad i = 0, 1, 2, 3, 4, 5, 6, \tag{39}$$

$$\{\kappa\} = \begin{Bmatrix} \kappa_{xx} \\ \kappa_{yy} \\ 2\kappa_{xy} \\ 2\kappa_{xz} \\ 2\kappa_{yz} \end{Bmatrix} = \begin{Bmatrix} \theta_{x,x} \\ \theta_{y,y} \\ \theta_{y,x} + \theta_{x,y} \\ 0 \\ 0 \end{Bmatrix} = [H_2]\{\theta\}, \tag{40}$$

$$\{\varphi\} = \begin{Bmatrix} \varphi_{xx} \\ \varphi_{yy} \\ 2\varphi_{xy} \\ 2\varphi_{xz} \\ 2\varphi_{yz} \end{Bmatrix} = \begin{Bmatrix} 0 \\ 0 \\ 0 \\ \theta_x + w_{0,x} \\ \theta_y + w_{0,y} \end{Bmatrix} = [H_3]\{\theta\}, \tag{41}$$

$$\{\psi\} = \begin{Bmatrix} \psi_{xx} \\ \psi_{yy} \\ 2\psi_{xy} \\ 2\psi_{xz} \\ 2\psi_{yz} \end{Bmatrix} = \begin{Bmatrix} \theta_{x,x} \\ \theta_{y,y} + w_{,yy} \\ \theta_{x,y} + \theta_{y,x} + 2 * w_{,xy} \\ 0 \\ 0 \end{Bmatrix} = [H_4]\{\theta\}. \tag{42}$$

On the other hand, δW_{ext} is given by:

$$\delta W_{ext} = \lambda(t) \int \left(\{\delta q\}^T \{F_e\} + \{\delta\theta\}^T \{M_e\} \right) dS, \tag{43}$$

where $\lambda(t)$ is a loading parameter depend on time, F_e is the force vector expressed by $\{F_e\}^T = \langle F_x, F_y, F_z \rangle$ and $\{M_e\}$ is the moment vector given by $\{M_e\}^T = \langle 0, 0, 0, 0, 0, 0, M_x, M_y, 0, 0, 0, 0, 0, 0, 0 \rangle$.

Taking into account the equations (33), (38) and (39), the Hamilton's principle is written in the form:

$$\begin{aligned} \int \langle \delta U \rangle [M] \{\ddot{U}\} dS + \int \Big(& \langle \delta\varepsilon \rangle [D_0] \{\varepsilon\} + \langle \delta\kappa \rangle [D_1] \{\varepsilon\} - 3c \langle \delta\varphi \rangle [D_2] \{\varepsilon\} \\ & - c \langle \delta\psi \rangle [D_3] \{\varepsilon\} + \langle \delta\varepsilon \rangle [D_1] \{\kappa\} + \langle \delta\kappa \rangle [D_2] \{\kappa\} - 3c \langle \delta\varphi \rangle [D_3] \{\kappa\} \\ & - c \langle \delta\psi \rangle [D_4] \{\kappa\} - 3 \langle \delta\varepsilon \rangle [D_2] \{\varphi\} - 3c \langle \delta\kappa \rangle [D_3] \{\varphi\} \\ & + 9c^2 \langle \delta\varphi \rangle [D_4] \{\varphi\} + 3c^2 \langle \delta\psi \rangle [D_5] \{\varphi\} - c \langle \delta\varepsilon \rangle [D_3] \{\psi\} - c \langle \delta\kappa \rangle [D_4] \{\psi\} \\ & + 3c^2 \langle \delta\varphi \rangle [D_5] \{\psi\} + c^2 \langle \delta\psi \rangle [D_6] \{\psi\} \Big) dS = \lambda(t) \int \left(\{\delta q\}^T \{F_e\} + \{\delta\theta\}^T \{M_e\} \right) dS. \end{aligned} \tag{44}$$

4.1. Discretization with the finite element method

Spatial discretization is performed by the finite element method which consists to discretize the domain S into several subdomains S_e called element. The displacements $\{U\}$ are related with the nodal displacements $\{r\}^e$ on each element via a matrix $[N]$ of interpolation functions, as follows $\{U\} = [N]\{r\}^e$. Likewise, the displacement gradient vector $\{\theta\}$ is expressed as a function of the nodal displacements $\{r\}^e$ via a matrix $[G]$ of gradients of interpolation functions, as follows $\{\theta\} = [G]\{r\}^e$. Note that there is seven degrees of freedom per node, four independent components $(u, v, \theta_x, \theta_y)$, the transverse displacement w and its derivatives (w_x, w_x). To ensure a good approximation, for interpolation functions, we adopt bilinear Lagrange functions for axial displacements $(u,\ v)$ and rotations (θ_x, θ_y) and high degree Hermite functions for the transverse displacement w. In this work, we choose the quadrilateral element which is the optimal choice. The passage of the reference elements to the real elements is carried out by a geometric transformation which is called "Jacobian transformation". Consider the coordinates of the real elements x and y and the coordinates of the reference elements ξ and η, so we

can write:

$$\begin{cases} x = \sum\limits_{i=1}^{nn} N_i(\xi,\eta)x_i, \\ y = \sum\limits_{i=1}^{nn} N_i(\xi,\eta)y_i. \end{cases} \tag{45}$$

Where nn is the number of nodes per element.

After the spatial discretization, the tensors $\{\varepsilon\}$, $\{\kappa\}$, $\{\varphi\}$, and $\{\psi\}$ can be written in the following forms:

$$\{\varepsilon\} = [H_1][G]\{r^e\} + \frac{1}{2}[A(\theta)][G]\{r^e\} = [B_1(\theta)]\{r^e\}, \tag{46}$$

where $[B_1(\theta)] = [B^l] + [B^{nl}]$,

$$\{\kappa\} = [H_2][G]\{r^e\} = [B_2]\{r^e\}, \tag{47}$$

$$\{\varphi\} = [H_3][G]\{r^e\} = [B_3]\{r^e\}, \tag{48}$$

$$\{\psi\} = [H_4][G]\{r^e\} = [B_4]\{r^e\}. \tag{49}$$

Injecting these expressions above in the Hamilton's principle equation, one can get the following equations of motion:

$$\begin{aligned} \sum_{e=1}^{ne}\int \Big([B_1(\theta)]^T[D_0]\{\varepsilon\} + [B_2]^T[D_1]\{\varepsilon\} - 3c[B_3]^T[D_2]\{\varepsilon\} \\ - c[B_4]^T[D_3]\{\varepsilon\} + [B_1(\theta)]^T[D_1]\{\kappa\} + [B_2]^T[D_2]\{\kappa\} \\ - 3c[B_3]^T[D_3]\{\kappa\} - c[B_4]^T[D_4]\{\kappa\} - 3c[B_1(\theta)]^T[D_2]\{\varphi\} \\ - 3c[B_2]^T[D_3]\{\varphi\} + 9c^2[B_3]^T[D_4]\{\varphi\} + 3c^2[B_4]^T[D_5]\{\varphi\} \\ - c[B_1(\theta)]^T[D_3]\{\psi\} - c[B_2]^T[D_4]\{\psi\} + 3c^2[B_3]^T[D_5]\{\psi\} + c^2[B_4]^T[D_6]\{\psi\}\Big)dS \\ + \sum_{e=1}^{ne}\int [N_2]^T[M][N_2]\{\ddot{r^e}\}dS_e = \sum_{e=1}^{ne}\lambda(t)\int \{\delta r^e\}\Big([N_1]^T\{F_e\} + [G]^T\{M_e\}\Big)dS_e, \end{aligned} \tag{50}$$

where ne is the total number of elements. Using the assembly technique, equations of motion can be rewritten in the following global form:

$$\left[M_g\right]\{\ddot{r}\} + \left[K_g(\theta)\right]\{r\} = \lambda(t)\{F_g\}. \tag{51}$$

4.2. Eigenvalue equations

The theoretical formulation of free vibration is the same as nonlinear vibration, except that the strain tensor must be linear and the work of the external forces is zero. To determine the eigenmodes, we assume that the displacement field can be written in the following form:

$$\{r\} = \{\varnothing\}\cos(\omega t), \tag{52}$$

where $\varnothing$ is a vector which corresponds to a mode. We inject the approximation (52) in the equation (51) to obtain the following equation:

$$\left(-\omega^2\left[M_g\right] + \left[K_{gl}\right]\right)\{\varnothing\} = \{0\}, \tag{53}$$

where $\left[K_{gl}\right]$ is the linear part of the stiffness matrix. This is the eigenvalue problem where the existence of solution to matrix equation (53) leads to:

$$\det(M^{-1}K - \omega^2 I) = 0. \tag{54}$$

5. Numerical result

In this numerical section, we are interested to determine the natural frequencies of each FGM plate and to examine the influence of the exponent N which represents the variation of the material properties of P-FGM and S-FGM plates. In addition, we determinate the natural frequencies of E-FGM plates and examine the influence of the thickness on this kind of plates. In this study, the effect of different boundary conditions has been taken into account as shown in Fig. 5, material properties of FGM plate given in Table 1 are used, and the obtained numerical results are compared with those given in references [18] and [16] in particular case of P-FGM plates.

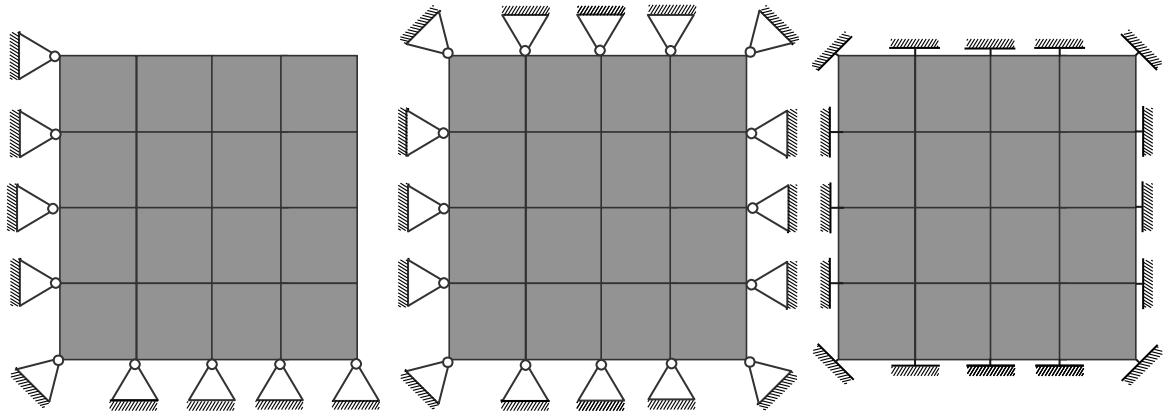

Fig. 5. Different boundary conditions SSFF, SSSS and CCCC.

Table 1. Material properties of FGM plate.

Material characteristics	E (GPa)	ν	ρ (Kg/m^3)
Metal material ($Ti-6Al-4V$)	122.56	0.31	4429
Ceramic material ($Zro2$)	244.27	0.288	3000

5.1. Influence of the exponent N of the volume fraction for P-FGM and S-FGM plates

In this part, we examine the influence of the exponent N of the volume fraction for P-FGM and S-FGM. We consider a simply supported square plate $SSSS$ (see Fig. 5-(B)) of side 0.2 m with uniform thickness $h = 0.025$ m and material properties given in Table 1. Note that the Poisson's ratio of the FGM plate is considered constant and equal to the average of the given coefficients for two materials. The plate is discretized by 5×5 elements. The eigen-frequencies have been calculated by the proposed approach for a square P-FGM plate and compared with the results of references [16] and [18] as shown in Table 2. Table 3 presents the calculated eigen-frequencies by the proposed approach for a square S-FGM. These results show that when the exponent N increases the frequencies decrease.

In Fig. 6, the first eight eigen-frequencies of the P-FGM plate and the S-FGM plate are illustrated. We notice that the results of the P-FGM plate are very close to those obtained with the S-FGM plate. Also note that the fundamental frequencies depend on the volume fraction of materials of FGM plates.

5.2. Influence of the length-to-thickness ratio ($a/h = b/h$) of the E-FGM plates

Consider three E-FGM plates of the same proprieties material with different aspect ratios (length/thickness): Plate 1 with $a/h = b/h = 4$, plate 2 with $a/h = b/h = 8$, and plate 3 with $a/h = b/h = 12$, knowing that $a = b = 0.2$ m. There are the same discretization 5×5 elements and the same boundary conditions of a simply supported square plate $SSSS$ (see Fig. 5-(B)) as in the previous

Table 2. Eigen-frequencies of free vibration of a square P-FGM plate.

Mode	Reference	N=0	N=0.5	N=1	N=2	Nε[300, ∞]	E-FGM
(1.1)	[18]	8.270	7.130	6.657	6.286	–	–
	TSDT [16]	8.968	7.530	6.980	6.513	–	–
	CPT [16]	9. 723	8.073	7.2429	6.930	–	–
	present	9.276	7.8	7.2022	6.6362	5.4253	4.1805
(1.2)	[18]	19.261	16.643	15.514	14.625	–	–
	TSDT [16]	21.276	17.871	16.551	15.413	–	–
	CPT [16]	24.235	20.093	18.465	17.212	–	–
	Present	19.5621	17.27	15.8446	14.5588	11.3521	8.8075
(1.3)	[18]	34.870	30.174	28.120	26.454	–	–
	TSDT [16]	36.343	30.813	28.276	25.850	–	–
	CPT [16]	36.34	30.827	28.296	25.867	–	–
	present	32.8	30.23	27.7465	25.4818	18.8694	15.1051

Table 3. Eigenfrequencies of free vibration of a square S-FGM plate.

Mode	$N = 0.5$	$N = 1$	$N = 2$	$N = 3$	$N_{max} = 70$	E-FGM
(1.1)	8.1466	7.3047	6.6754	6.4125	4.9332	4.1805
(1.2)	17.2766	15.51192	14.1992	13.6463	10.3765	8.8075
(1.3)	29.7124	26.7584	24.5242	23.5847	27.8321	15.1051

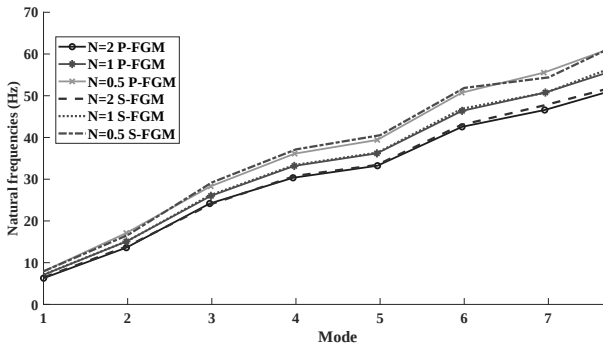

Fig. 6. Comparison of the natural frequencies between the P-FGM plate and the S-FGM plate.

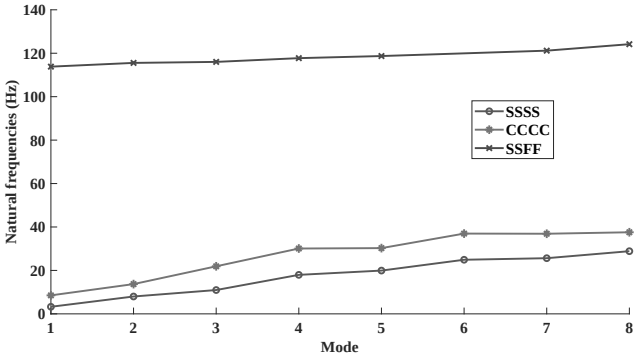

Fig. 7. Eigenfrequencies of free vibration of a square of a E-FGM plate with various boundary conditions.

example in the section 5.1. We present in Table 4 the first three eigen-frequencies of three plates 1, 2 and 3. This table shows that increasing the length-to-thickness ratio decreases the fundamental frequencies. This means that the stiffness of the E-FGM plate decreases with increasing aspect ratio (length/thickness).

Fig. 7 shows the proportionality of the fundamental frequencies with the vibrational modes of E-FGM plates. These fundamental frequencies become significant for higher fundamental vibrational modes. From this figure, we also conclude that the fundamental frequencies depend on the boundary conditions type. The fundamental frequencies of the plate $CCCC$ are a little bigger than those of the plate $SSSS$. On the other hand, the fundamental frequencies of the plate $SSFF$ are much larger than those of the plate $SSSS$ and the plate $CCCC$.

Table 4. Eigen-frequencies of free vibration of a square E-FGM plate with different aspect ratios (length/thickness).

Mode	$a/h = b/h = 4$	$a/h = b/h = 8$	$a/h = b/h = 12$
(1.1)	7.2654	4.1805	2.8985
(1.2)	14.4294	8.8075	6.2119
(1.3)	23.1815	15.1051	10.8800

Other results are presented in the appendices in Figs. 8 and 9 to compare the results of simple FGM plates with those of laminated FGM plates. For laminated FGM plates, materials are joined as in laminated composite materials. For simple P-FGM plates, the Poisson's ratio is the average of those of two materials (ceramic/metal) using the power law.

6. Conclusion

Free vibrations of the FGM plates using the third-order theory (TSDT) are studied in this paper. We considered that the material properties change continuously through the thickness of the plate following the different laws which represent the variation of FGM properties, namely: the exponential law (E-FGM), the power-law (P-FGM), and the sigmoid law (S-FGM). Using the Hamilton's principle and the finite element method with four nodes per element, we obtained the equations of motion and then the eigenvalue equations. Solving these equations allows us to calculate the eigen-frequencies and the eigenmodes. We conclude that the change of the fundamental frequencies depends on the type of law of the volume fraction of materials. This is remarkable when comparing results obtained on for two plates S-FGM and P-FGM. The results also show that the power law and the sigmoid law give roughly the same eigen-frequencies. The study of the influence of the exponent N for the S-FGM plate and the P-FGM plate shows that when N increases we observe the increase of the natural frequencies. This means that the FGM plates have the advantage of improving material stiffness. In addition, the study of the influence of the aspect ratio (length/thickness) of the E-FGM plates explains that increasing of the aspect ratio decreases the fundamental frequencies. Other results are presented in the appendices, these results show that laminated FGM plates give the natural frequencies lower than those of simple FGM plates, the difference between them increases according to the number of modes. The objective in the future is to apply this approach on other type of shells, such as FGM cylindrical Shells [15, 19]. In addition, we will try to develop meshless models [20–27] based on TSDT theory for the analysis of FGM plates.

7. Appendices

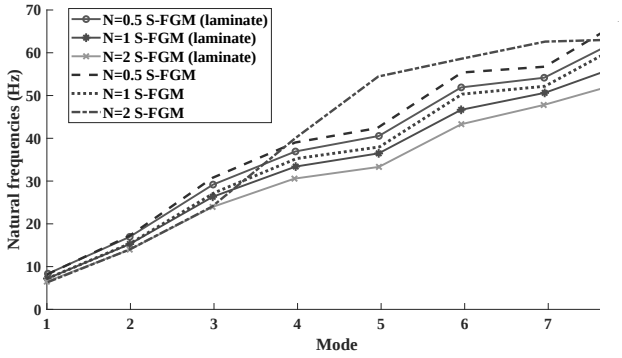

Fig. 8. Comparison of natural frequencies between a laminated S-FGM plate and a simple S-FGM plate using the sigmoid law.

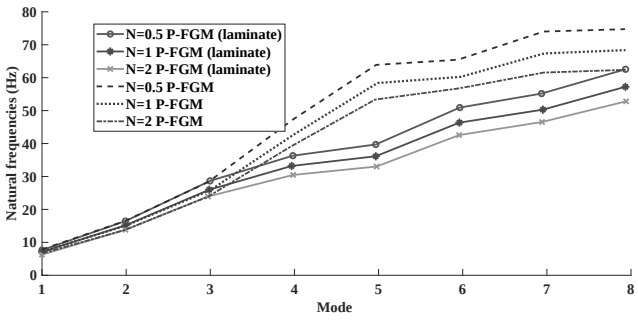

Fig. 9. Comparison of natural frequencies between a laminated P-FGM plate and a simple P-FGM plate using the power law.

[1] Vinh P. V., Dung N. T., Tho N. C., Thom D. V., Hoa L. K. Modified single variable shear deformation plate theory for free vibration analysis of rectangular FGM plates. Structures. **29**, 1435–1444 (2021).

[2] Auada S. P., Pracianoa J. S. C., Barrosoa E. S., Sousa Jr J. B. M., Parente Juniora E. Isogeometric Analysis of FGM Plates. Materials Today: Proceedings. **8** (3), 738–746 (2019).

[3] Kim S. E., Duc N. D., Nam V. H., Van Sy N. Nonlinear vibration and dynamic buckling of eccentrically oblique stiffened FGM plates resting on elastic foundations in thermal environment. Thin-Walled Structures. **142**, 287–296 (2019).

[4] Fu T., Chen Z., Yu H., Wang Z., Liu X. An analytical study of sound transmission through corrugated core FGM sandwich plates filled with porous material. Composites Part B: Engineering, **151**, 161–172 (2018).

[5] Sharma P., Meena M., Khinchi A. Modal study of bi direction FGM plate. Materials Today: Proceedings. **44** (1), 1604–1608 (2021).

[6] Kar U. K., Srinivas J. Material modeling and analysis of hydroxyapatite/titanium FGM plate under thermo-mechanical loading conditions. Materials Today: Proceedings. **33** (8), 5498–5504 (2020).

[7] Katili I., Batoz J. L., Maknun I. J., Katili A. M. On static and free vibration analysis of FGM plates using an efficient quadrilateral finite element based on DSPM. Composite Structures. **261**, 113514 (2021).

[8] Zheng H., Sladek J., Sladek V., Wang S. K., Wen P. H. Hybrid meshless/displacement discontinuity method for FGM Reissner's plate with cracks. Applied Mathematical Modelling. **90**, 1226–1244 (2021).

[9] Hassan A. H. A., Kurgan N. Bending analysis of thin FGM skew plate resting on Winkler elastic foundation using multi-term extended Kantorovich method. Engineering Science and Technology, an International Journal. **23** (4), 788–800 (2020).

[10] Yang H. S., Dong C. Y., Wu Y. H. Postbuckling analysis of multi-directional perforated FGM plates using NURBS-based IGA and FCM. Applied Mathematical Modelling. **84**, 466–500 (2020).

[11] Minh P. P., Manh D. T., Duc N. D. Free vibration of cracked FGM plates with variable thickness resting on elastic foundations. Thin-Walled Structures. **161**, 107425 (2021).

[12] Li M., Yan R., Xu L., Guedes Soares C. A general framework of higher-order shear deformation theories with a novel unified plate model for composite laminated and FGM plates. Composite Structures. **261**, 113560 (2021).

[13] Minh P. P., Duc N. D. The effect of cracks and thermal environment on free vibration of FGM plates. Thin-Walled Structures. **159**, 107291 (2021).

[14] Tran T. T., Nguyen P. C., Pham Q. H. Vibration analysis of FGM plate in thermal environment resting on elastic foundation using ES-MITC3 element and prediction of ANN. Case Studies in Thermal Engineering. **24**, 100852 (2021).

[15] Timesli A. Analytical Modeling of Buckling Behavior of Porous FGM Cylindrical Shell Embedded within an Elastic Foundation. Gazi University Journal of Science (2021).

[16] Bourihane O., Hilali Y., Mhada K. Nonlinear dynamic response of functionally graded material plates using a high-order implicit algorithm. Journal of Applied Mathematics and Mechanics. **100** (12), e202000087 (2020).

[17] Ghatage P. S., Kar V. R., Sudhagar P. E. On the numerical modelling and analysis of multi-directional functionally graded composite structures: A review. Composite Structures. **236**, 111837 (2020).

[18] Huang X. L., Shen H. S. Nonlinear vibration and dynamic response of functionally graded plates in thermal environments. International Journal of Solids and Structures. **41** (9–10), 2403–2427 (2004).

[19] Timesli A. Prediction of the critical buckling load of SWCNT reinforced concrete cylindrical shell embedded in an elastic foundation. Computer and Concrete. **26** (1), 53–62 (2020).

[20] Saffah Z., Timesli A., Lahmam H., Azouani A., Amdi M. New collocation path-following approach for the optimal shape parameter using Kernel method. SN Applied Sciences. **3**, Article number: 249 (2021).

[21] Timesli A., Braikat B., Lahmam H., Zahrouni H. An implicit algorithm based on continuous moving least square to simulate material mixing in friction stir welding process. Modelling and Simulation in Engineering. **2013**, Article ID: 716383, 1–14 (2013).

[22] Timesli A. Optimized radius of influence domain in meshless approach for modeling of large deformation problems. Iranian Journal of Science and Technology-Transactions of Mechanical Engineering (2021).

[23] Mesmoudi S., Timesli A., Braikat B., Lahmam H., Zahrouni H. A 2D mechanical-thermal coupled model to simulate material mixing observed in friction stir welding process. Engineering with Computers. **33**, 885–895 (2017).

[24] Timesli A, Braikat B., Lahmam H., Zahrouni H. A new algorithm based on Moving Least Square method to simulate material mixing in friction stir welding. Engineering Analysis with Boundary Elements. **50**, 372–380 (2015).

[25] Belaasilia Y, Timesli A, Braikat B, Jamal M. A numerical mesh-free model for elasto-plastic contact problems. Engineering Analysis with Boundary Elements. **82**, 68–78 (2017).

[26] El Kadmiri R., Belaasilia Y., Timesli A., Kadiri M. S. A coupled Meshless-FEM method based on strong-form of Radial Point Interpolation Method (RPIM). Journal of Physics: Conference Series, **1743**, 012039 (2021).

[27] El Kadmiri R., Belaasilia Y., Timesli A., Kadiri M. S. Meshless approach based on MLS with additional constraints for large deformation analysis. Journal of Physics: Conference Series. **1743**, 012015 (2021).

Теорія ДЗТП для вільних коливань функціонально градієнтних пластин з різними властивостями матеріалів

Джанане Аллах М., Белаасиліа Й., Таймслі А., Ель Хаузі А.

Університет Касабланки Хасана II,
Національна вища школа мистецтв та ремесел (ENSAM Касабланка),
20670 Касабланка, Марокко

У цій роботі використовується неявний алгоритм для аналізу вільної динамічної поведінки пластин із функціонально модифікованим матеріалом (ФММ). Теорія деформації зсуву третього порядку (ТДЗТП) використовується для розробки запропонованої моделі. У цій статті постановка здійснена без застосування гомогенізації суміші, яке, як правило, проводиться в такого роду задачах. Принцип Гамільтона використовується для отримання результуючих рівнянь руху. Для просторової дискретизації на основі методу скінчених елементів (МСЕ), приймається квадратичний елемент із чотирма та вісьмома вузлами із використанням семи ступенів свободи на вузол. Для розв'язання отриманої задачі використовується неявний алгоритм. Для вивчення точності та ефективності запропонованого підходу подано порівняння з даними, наведеними в літературі та результатами моделювання композитного ламінату для власних частот вібрацій. Інакше кажучи, ми дослідили вплив показника об'ємної частки, на яку реагують пластини "П-ФММ" та "С-ФММ". Більше того, вивчтуj вплив товщини на пластини "Е-ФММ".

Ключові слова: *теорія деформації зсуву третього порядку (ТДЗТП), нелінійний динамічний аналіз, багатошаровий композит, функціонально модифікований матеріал (ФММ).*